A state space boundary element method with analytical nearly singular integral formulation

†Changzheng Cheng[1], *Zhilin Han[1], Meng Wu[2], Zhongrong Niu[1], Hongyu Sheng[1]

[1] School of Civil Engineering, Hefei University of Technology, Hefei 230009, PR China;
[2] School of Mathematics, Hefei University of Technology, Hefei 230009, PR China

*Presenting author: han_zhilin@mail.hfut.edu.cn
†Corresponding author: changzheng.cheng@hfut.edu.cn

Abstract:
A new method named the state space boundary element method (SSBEM) is established, in which the problem domain is divided into two parts. One is the boundary element domain which includes the interested inner point and the other is the state space domain. The boundary integral equation and state space equation are combined together by the interfacial continuity condition to form the system equation of the SSBEM. The SSBEM synthesizes both advantages of the boundary element method and state space method, while it will get inaccurate result when it is used to evaluate the mechanical quantity of the point very close to the boundary element, because the Gaussian's quadrature fails to calculate the nearly singular integral in the boundary integral equation. The analytical formulation developed by part of the authors before is introduced to deal with the nearly singular integral. Thus, the SSBEM can yield accurate physical quantities for the point very close to the boundary element. The SSBEM result can well agree with the one from the finite element method (FEM), while the discretized element is much less than the one in the FEM. Meanwhile, the SSBEM can analyze very thin coating while the FEM fails due to the limitation of Boolean operation tolerance.

Keywords: state space method, boundary element method, nearly singular integral, analytical formulation

1. Introduction

The state space method (SSM) is widely used in the analysis of laminated structure because of its simple recursive formulation [1]. According to different discretization method of in-plane variables, the SSM can be summarized as four types, which are the finite strip SSM [2]-[4], the finite element SSM [5]-[7], the differential quadrature SSM [8] and the meshless SSM [9]-[11]. Since only in-plane interfaces are meshed, the SSM can decrease the element number when they are compared with the finite element method (FEM). However, when an interested inner point is designated to be analyzed, the structure has to be delaminated into more sub-layers to ensure that the interior point is exactly located on the interface which undoubtedly increases the computational cost.

The boundary element method (BEM) is based on the classical integral equation formulation

of boundary value problem [12]-[15]. The unknown physical quantity at any interior point can be directly evaluated by the boundary integral equation. The experience has shown that the BEM has advantages over other numerical methods for reducing the calculation amount. However, the sub-domain method has to be introduced when it comes to the laminated structure, which will increase the redundant interface quantity in the BEM.

By coupling two independent methods, their respective merits can be enlarged and shortcomings can be overcome. There are some direct coupling techniques, such as the BEM-BEM method [16][17], the FEM-BEM method [18]-[20], fast multipole BEM-SSM method [21], etc. There is also an iterative coupling technique [22]-[24] developed in the FEM-BEM method, which provides a novel calculative strategy for the coupled method. Herein, the BEM-SSM coupling method named the state space boundary element method (SSBEM) is developed basing on the direct coupling technique, which can efficiently analyze the laminated structure and easily yield the physical quantity of the inner point without increasing the amount of calculation.

It should be pointed out that the integral kernel in the boundary integral equation will present nearly singularity when the distance from the source point to the field point is close to but not equal to zero. The accuracy of SSBEM, such as the evaluation of the near boundary inner point, depends on the accurate evaluation of nearly singular integral significantly. The analytical formulation for the nearly singular integral proposed by part of the authors before [25] is introduced to the SSBEM, which can be used to calculate the physical quantity for near boundary interior point accurately.

2. Boundary integral equation with analytical nearly singular integral formulation

The thermal elasticity problem is considered here, which can be degenerated to the elasticity problem if the temperature loading is set as zero. The displacement boundary integral equation with respect to the source point $\boldsymbol{y}$ for two-dimensional thermal elasticity problem can be written as

$$C_{ij}(\boldsymbol{y})u_j(\boldsymbol{y}) = \int_\Gamma [U_{ij}^* t_j(\boldsymbol{x}) - T_{ij}^* u_j(\boldsymbol{x})]\mathrm{d}\Gamma + \int_\Gamma [R_i^* T(\boldsymbol{x}) - Q_i^* \partial T(\boldsymbol{x})/\partial n]\mathrm{d}\Gamma \tag{1}$$

where $\boldsymbol{x}$ is the field point, $i, j = 1, 2$ respectively denote the direction along *x*- and *y*-axis in the rectangular coordinate system. $C_{ij}(\boldsymbol{y})$ is the coefficient determined by the local geometry at point $\boldsymbol{y}$. $u_j(\boldsymbol{x})$ and $t_j(\boldsymbol{x})$ are, respectively, the displacement and traction on the boundary Γ of the structure. $T(\boldsymbol{x})$ and $\partial T(\boldsymbol{x})/\partial n$ are the temperature and temperature gradient at point $\boldsymbol{x}$, respectively. U_{ij}^* and T_{ij}^* are the fundamental solutions for governing equation of elasticity, for the plane strain problem which can be written as

$$U_{ij}^{*}=\frac{1}{8\pi(1-\nu)G}[(3-4\nu)\ln r\delta_{ij}-\frac{r_i r_j}{r^2}] \tag{2a}$$

$$T_{ij}^{*}=\frac{1}{4\pi(1-\nu)}[(1-2\nu)(\frac{r_i n_j-r_j n_i-r_n\delta_{ij}}{r^2})-\frac{2r_i r_j r_n}{r^4}] \tag{2b}$$

where δ_{ij} is the Kronecker symbol, G is the shear modulus and ν is the Poisson's ratio. $r_i=x_i-y_i$ and $r=(r_i r_i)^{1/2}$ is the distance between the field point and source point. R_i^{*} and Q_i^{*} in Eq. (1) are the fundamental solutions related to the thermal elasticity governing equation, which can be written as

$$R_i^{*}=\frac{\alpha(1+\nu)}{4\pi(1-\nu)}[(\ln\frac{1}{r}-\frac{1}{2})n_i-\frac{r_i r_n}{r^2}] \tag{3a}$$

$$Q_i^{*}=\frac{\alpha(1+\nu)}{4\pi(1-\nu)}(\ln\frac{1}{r}-\frac{1}{2})r_i \tag{3b}$$

where α is the thermal expansion coefficient.

By discretizing Eq.(1) along the boundary, the boundary element method system equation can be yielded like

$$\boldsymbol{Hu}=\boldsymbol{Gt} \tag{4}$$

where $\boldsymbol{H}$ and $\boldsymbol{G}$ are coefficient matrices, $\boldsymbol{u}$ is nodal displacement vector and $\boldsymbol{t}$ is nodal traction vector.

After the unknown displacement and traction on the boundary Γ being solved from Eq. (4), the displacement at any interior point can be evaluated by the displacement boundary integral equation

$$u_i(\boldsymbol{y})=\int_\Gamma[U_{ij}^{*}t_j(\boldsymbol{x})-T_{ij}^{*}u_j(\boldsymbol{x})]\mathrm{d}\Gamma+\int_\Gamma[R_i^{*}T(\boldsymbol{x})-Q_i^{*}\,\partial T(\boldsymbol{x})/\partial n]\mathrm{d}\Gamma \tag{5}$$

By taking the derivative of Eq. (5) and introducing the strain-stress relationship, the stress at any interior point can be expressed by the stress boundary integral equation

$$\sigma_{ij}(\boldsymbol{y})=\int_\Gamma[W_{ijk}^{*}t_k(\boldsymbol{x})-S_{ijk}^{*}u_k(\boldsymbol{x})]\mathrm{d}\Gamma+\int_\Gamma[R_{ij}^{*}T(\boldsymbol{x})-Q_{ij}^{*}\partial T(\boldsymbol{x})/\partial n]\mathrm{d}\Gamma-\sigma_{ij}^{0}(\boldsymbol{y}) \tag{6}$$

where $i,j,k=1,2$, $\sigma_{ij}^{0}(\boldsymbol{y})=2G(1+\nu)\alpha\cdot\Delta T(\boldsymbol{y})\delta_{ij}/(1-2\nu)$ and the integral kernels are listed as follows

$$W_{ijk}^{*}=\frac{1}{4\pi(1-\nu)}[(1-2\nu)\frac{r_i\delta_{jk}+r_j\delta_{ik}-r_k\delta_{ij}}{r^2}+\frac{2r_i r_j r_k}{r^4}] \tag{7a}$$

$$S_{ijk}^{*}=\frac{G}{2\pi(1-\nu)}[\frac{(1-2\nu)(n_i\delta_{jk}+n_j\delta_{ki})-(1-4\nu)n_k\delta_{ij}}{r^2}-\frac{4r_n r_i r_j r_k}{r^6}+\frac{2(1-2\nu)(r_n r_k\delta_{ij}+r_i r_j n_k)+2\nu(r_n r_j\delta_{jk}+r_n r_j\delta_{ik}+n_i n_j r_k+n_j r_i r_k}{r^4}] \tag{7b}$$

$$R_{ij}^{*}=\frac{G\alpha(1+\nu)}{2\pi(1-\nu)}[\frac{r_n\delta_{ij}/(1-2\nu)+n_i r_j+n_j r_i}{r^2}-\frac{2r_i r_j r_n}{r^4}] \tag{7c}$$

$$Q_{ij}^{*}=\frac{G\alpha(1+\nu)}{2\pi(1-\nu)}[\frac{r_i r_j}{r^2}-\frac{1}{1-2\nu}(\ln\frac{1}{r}-\frac{1+2\nu}{2})\delta_{ij}] \tag{7d}$$

It can be observed that the integral kernels shown in Eqs. (2,3) and Eq. (7) contain nearly singular items of order $O(1/r^2)$, $O(1/r^4)$ and $O(1/r^6)$. When the source point is close to the integral element, the implementation with Gaussian's quadrature will lead to significant inaccuracy in obtaining the results of nearly singular integral.

The integrals in Eqs. (1,5,6) can be concluded as three kinds of forms as follows

$$I_1=\int_{-1}^{1}\frac{P_1(\xi)}{R}\mathrm{d}\xi,\quad I_2=\int_{-1}^{1}\frac{P_2(\xi)}{R^2}\mathrm{d}\xi,\quad I_3=\int_{-1}^{1}\frac{P_3(\xi)}{R^4}\mathrm{d}\xi \tag{8}$$

where $R=r^2$, $P_1(\xi)$, $P_2(\xi)$ and $P_3(\xi)$ are the polynomial functions of local coordinate ξ. By means of integration by parts, Eq. (8) is transformed into the analytical formulation [25] as follows

$$\begin{aligned}I_1=&\{\frac{2}{\delta}P_1 g-\frac{1}{a}P_1'[(\frac{R'}{\delta})g-\frac{1}{2}\ln(\delta^2+R'^2)]+\frac{\delta}{4a^2}P_1''[(\frac{R'}{\delta})^2 g-\frac{R'}{\delta}+g]-\\&\frac{\delta^2}{8a^3}P_1'''\ (K_0+K_2-\frac{2aR}{\delta^2})\}\ \Big|_{\xi=-1}^{1}-\frac{1}{2a}\int_{-1}^{1}P_1''\ln(\delta^2+R'^2)\,\mathrm{d}\xi\\&+\frac{\delta^2}{8a^3}\int_{-1}^{1}P_1^{(4)}(K_0+K_2-\frac{2aR}{\delta^2})\ \mathrm{d}\xi\end{aligned} \tag{9a}$$

$$\begin{aligned}I_2=&\{\frac{1}{\delta^2}\frac{R'}{R}P_2+\frac{2}{\delta^3}(2aP_2-R'P_2')g+\frac{1}{2a\delta}P_2''[(\frac{R'}{\delta})^2 g+g-\frac{R'}{\delta}]\\&-\frac{1}{4a^2}P_2'''(K_0+K_2-\frac{2aR}{\delta^2})+\frac{\delta}{8a^3}P_2^{(4)}(K_1+\frac{1}{3}K_3)\}\ \Big|_{\xi=-1}^{1}\\&-\frac{1}{4a^2}\int_{-1}^{1}P_2^{(4)}[\frac{2aR}{\delta^2}+\frac{1}{6}(\frac{R'}{\delta})^2+\frac{1}{3}\ln(\delta^2+R'^2)-\frac{2}{3}\ln\delta\,]\mathrm{d}\xi\\&-\frac{\delta}{8a^3}\int_{-1}^{1}P_2^{(5)}(K_1+\frac{1}{3}K_3)\mathrm{d}\xi\end{aligned} \tag{9b}$$

$$\begin{aligned}I_3=&\{\frac{R'}{2\delta^2R^2}P_3+\frac{R'}{2\delta^4R}(6aP_3-R'P_3')+\frac{1}{\delta^5}(12a^2P_3+\frac{3}{2}R'^2P_3''-6aR'P_3')g\\&+\frac{1}{2\delta^3}P_3''(g-\frac{R'}{\delta})+\frac{1}{4a\delta^2}P_3'''[\frac{2aR}{\delta^2}+\frac{1}{2}(\frac{R'}{\delta})^2-\frac{R'}{\delta}g-(\frac{R'}{\delta})^3 g]\\&+\frac{1}{32a^2\delta}P_3^{(4)}[(\frac{R'}{\delta})^4 g+2(\frac{R'}{\delta})^2 g+g-\frac{1}{3}(\frac{R'}{\delta})^3-\frac{R'}{\delta}\ ]\}\Big|_{\xi=-1}^{1}\\&-\frac{1}{4a\delta^2}\int_{-1}^{1}P_3^{(4)}[\frac{1}{2}(\frac{R'}{\delta})^2+\frac{2aR}{\delta^2}]\mathrm{d}\xi-\frac{1}{8\delta a^2}\int_{-1}^{1}P_3^{(5)}(K_1+K_3)\mathrm{d}\xi\end{aligned} \tag{9c}$$

where the prime and bracket in the superscript denote the partial derivatives to ξ, $K_n\,(n=0,1,2,3)$ are functions with respect to g, $g=\mathrm{arctg}(R'/\delta)$, $\delta=\sqrt{4ac-b^2}$, a, b and c are the expanded coefficients of r^2 in the local coordinate ξ, i.e.,

$$r^2=a\xi^2+b\xi+c \tag{10}$$

When the polynomial function whose order is lower than four is adopted, Eq.(9) is the analytical formulation.

3. State space equation with precise integral method

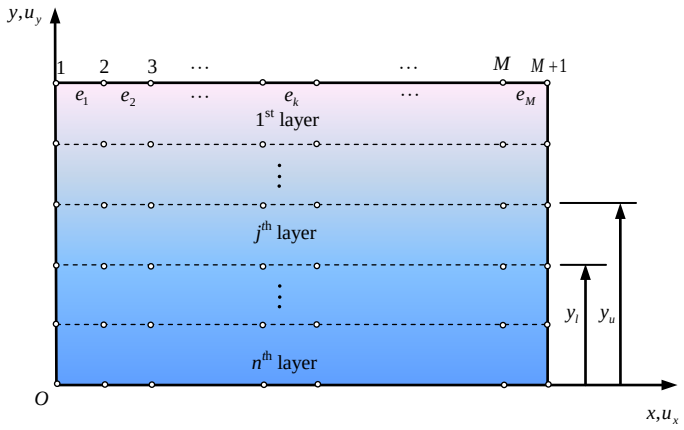

Fig.1 Discretization for laminated structure in the state space method

A laminated structure composed by n layers is considered here, see Fig.1, in which each layer could have different elastic modulus E and different thermal expansion coefficients α. On the basis of Hellinger-Reissner variational principle, the equilibrium equation and strain-displacement relation at any elastic layer shown in Fig. 1 can be equivalently written as

$$\iint_{\Omega} \delta \boldsymbol{u}^{\mathrm{T}} \left[\boldsymbol{E}(\nabla)\boldsymbol{\sigma} + \boldsymbol{f} \right] \mathrm{d}\Omega = 0 \tag{11a}$$

$$\iint_{\Omega} \delta \boldsymbol{\sigma}^{\mathrm{T}} \left[\boldsymbol{\varepsilon} - \boldsymbol{E}^{\mathrm{T}}(\nabla)\boldsymbol{u} \right] \mathrm{d}\Omega = 0 \tag{11b}$$

where $\boldsymbol{\varepsilon}$ and $\boldsymbol{\sigma}$ denote strain and stress vectors, respectively, $\boldsymbol{f}$ is the body force. $\boldsymbol{E}(\nabla)$ is the differential operator

$$\boldsymbol{E}(\nabla) = \begin{bmatrix} \partial/\partial x & 0 & \partial/\partial y \\ 0 & \partial/\partial y & \partial/\partial x \end{bmatrix} \tag{12}$$

For the thermal elasticity problem, the stress-strain relation can be written as

$$\boldsymbol{\varepsilon} = \boldsymbol{S}\boldsymbol{\sigma} + \boldsymbol{J} \tag{13}$$

where $\boldsymbol{J} = [\alpha \cdot \Delta T \ \alpha \cdot \Delta T \ 0]^{\mathrm{T}}$, ΔT is the temperature loading. The flexibility matrix $\boldsymbol{S}$ can be expressed as

$$\boldsymbol{S} = \begin{bmatrix} S_1 & S_2 & 0 \\ S_2 & S_1 & 0 \\ 0 & 0 & S_3 \end{bmatrix} \tag{14}$$

where $S_1 = 1/E$, $S_2 = -\nu/E$, $S_3 = 2(1+\nu)/E$.

After introducing the stress-strain relationship, Eq.(11) can be transformed into

$$\iint_{\Omega}\begin{Bmatrix}\delta u_x\\ \delta u_y\\ \delta\tau_{xy}\\ \delta\sigma_{yy}\end{Bmatrix}^{\mathrm{T}}\left(\begin{bmatrix}0&0&1&0\\0&0&0&1\\1&0&0&0\\0&1&0&0\end{bmatrix}\frac{\partial}{\partial y}\begin{Bmatrix}u_x\\ u_y\\ \sigma_{xy}\\ \sigma_{yy}\end{Bmatrix}-\begin{bmatrix}0&0&0&0\\0&0&-\partial/\partial x&0\\0&-\partial/\partial x&S_3&0\\0&0&0&S_1\end{bmatrix}\begin{Bmatrix}u_x\\ u_y\\ \sigma_{xy}\\ \sigma_{yy}\end{Bmatrix}+\begin{bmatrix}\partial/\partial x\\0\\0\\-S_2\end{bmatrix}\sigma_{xx}+\begin{bmatrix}0\\0\\0\\-\alpha\end{bmatrix}\Delta T\right)\mathrm{d}\Omega=0 \tag{15a}$$

$$\iint_{\Omega}\{\delta\sigma_{xx}\}^{\mathrm{T}}\left(S_1\sigma_{xx}-\begin{bmatrix}\partial/\partial x&0&0&-S_2\end{bmatrix}\begin{Bmatrix}u_x\\ u_y\\ \sigma_{xy}\\ \sigma_{yy}\end{Bmatrix}+\alpha\cdot\Delta T\right)\mathrm{d}\Omega=0 \tag{15b}$$

where u_x and u_y are the displacements along the $x-$axis and $y-$axis, respectively. The relationship between the traction and stress on the boundary or at the interface can be written as

$$t_x=\sigma_{xy},\quad t_y=\sigma_{yy} \tag{16}$$

In the state space method, only the horizontal interfaces are discretized and it is assumed that M linear elements are meshed on each interface as shown in Fig. 1. By integrating along the *x*-coordinate and considering Eq.(16), Eq.(15) can be written as

$$\int_y\begin{Bmatrix}\delta\boldsymbol{u}\\ \delta\boldsymbol{t}\end{Bmatrix}^{\mathrm{T}}\left(\boldsymbol{A}\frac{\mathrm{d}}{\mathrm{d}y}\begin{Bmatrix}\boldsymbol{u}\\ \boldsymbol{t}\end{Bmatrix}-\boldsymbol{B}\begin{Bmatrix}\boldsymbol{u}\\ \boldsymbol{t}\end{Bmatrix}+\boldsymbol{C}\boldsymbol{s}+\boldsymbol{M}\boldsymbol{T}\right)\mathrm{d}y=0 \tag{17a}$$

$$\int_y\{\delta\boldsymbol{s}\}^{\mathrm{T}}\left(\boldsymbol{D}\boldsymbol{s}-\boldsymbol{E}\begin{Bmatrix}\boldsymbol{u}\\ \boldsymbol{t}\end{Bmatrix}+\boldsymbol{N}\boldsymbol{T}\right)\mathrm{d}y=0 \tag{17b}$$

where $\boldsymbol{A}$, $\boldsymbol{B}$, $\boldsymbol{C}$, $\boldsymbol{D}$, $\boldsymbol{E}$, $\boldsymbol{M}$ and $\boldsymbol{N}$ are the coefficient matrices deduced from Eq.(15). The vector $\boldsymbol{s}$ and $\boldsymbol{T}$ are respectively composed of nodal stress σ_{xx} and nodal temperature variation.

By eliminating $\boldsymbol{s}$ from Eq. (17) and utilizing the variational principle, the state equation at any layer can be written as

$$\frac{\mathrm{d}\boldsymbol{R}}{\mathrm{d}y}=\boldsymbol{W}\boldsymbol{R}+\boldsymbol{B} \tag{18}$$

where the state variable $\boldsymbol{R}=\{\boldsymbol{u}^{\mathrm{T}}\ \boldsymbol{t}^{\mathrm{T}}\}^{\mathrm{T}}$, $\boldsymbol{W}=\boldsymbol{A}^{-1}(\boldsymbol{B}-\boldsymbol{C}\boldsymbol{D}^{-1}\boldsymbol{E})$, and the vector $\boldsymbol{B}=\boldsymbol{A}^{-1}(\boldsymbol{C}\boldsymbol{D}^{-1}\boldsymbol{N}-\boldsymbol{M})\boldsymbol{T}$, which is the term related to the temperature variation.

The precise integral method [26] is introduced to solve Eq. (18). Let's take the jth layer in Fig. 1 for example. If the jth layer is sufficiently thin, $\boldsymbol{R}_j(y)$ and $\boldsymbol{B}_j(y)$ in Eq. (18) can be approximated by $[\boldsymbol{R}_j(y_u)+\boldsymbol{R}_j(y_l)]/2$ and $[\boldsymbol{B}_j(y_u)+\boldsymbol{B}_j(y_l)]/2$, respectively, where y_u and

y_l are y-coordinates of the upper interface and lower interface of the jth layer, respectively. For the layer which is not thin enough, it can be divided into $K_j = 2^k$ sub-layers with uniform thickness and each sub-layer can be approximately calculated as a thin layer. For the ith sub-layer in the jth layer, Eq. (18) can be written in the integrated form as follows

$$\int_{(i-1)\Delta_j}^{i\Delta_j} \mathrm{d}\boldsymbol{R}_j^{(i)}(y) = \int_{(i-1)\Delta_j}^{i\Delta_j} \boldsymbol{W}_j \boldsymbol{R}_j^{(i)}(y)\mathrm{d}y + \int_{(i-1)\Delta_j}^{i\Delta_j} \boldsymbol{B}_j^{(i)}(y)\mathrm{d}y \tag{19}$$

where Δ_j is the thickness of each sub-layer. By utilizing the approximation in the ith sub-layer which is thin enough, Eq. (19) can be transformed into

$$(\boldsymbol{I}-\boldsymbol{O})\boldsymbol{R}_j^{(i)}(i\Delta_j) = (\boldsymbol{I}+\boldsymbol{O})\boldsymbol{R}_j^{(i)}((i-1)\Delta_j) + \boldsymbol{U}_j^{(i)} \tag{20}$$

where $\boldsymbol{O} = \Delta_j \boldsymbol{W}_j / 2$, $\boldsymbol{U}_j^{(i)} = \Delta_j[\boldsymbol{B}_j(i\Delta_j) + \boldsymbol{B}_j((i-1)\Delta_j)]/2$ and $\boldsymbol{I}$ is a unit matrix. By applying Eq. (20) to each sub-layer and using the continuity condition between the interface of two adjacent sub-layers, i.e.,

$$\boldsymbol{R}_j^{(i)}[(i-1)\Delta_j] = \boldsymbol{R}_j^{(i-1)}[(i-1)\Delta_j] \tag{21}$$

one can get

$$(\boldsymbol{I}-\boldsymbol{O})^{K_j}\boldsymbol{R}_j(y_l) = (\boldsymbol{I}+\boldsymbol{O})^{K_j}\boldsymbol{R}_j(0) + \sum_{i=1}^{K_j}(\boldsymbol{I}+\boldsymbol{O})^{K_j-i}(\boldsymbol{I}-\boldsymbol{O})^{i-1}\boldsymbol{U}_j^{(i)} \tag{22}$$

The matrices $(\boldsymbol{I}-\boldsymbol{O})^{K_j}$ and $(\boldsymbol{I}+\boldsymbol{O})^{K_j}$ can be calculated by using the iteration process. The calculation of the last item $\boldsymbol{U}_j = \sum_{i=1}^{K_j}(\boldsymbol{I}+\boldsymbol{O})^{K_j-i}(\boldsymbol{I}-\boldsymbol{O})^{i-1}\boldsymbol{U}_j^{(i)}$ in Eq. (22) need to use the identity $(\boldsymbol{I}-\boldsymbol{O})(\boldsymbol{I}+\boldsymbol{O}) = (\boldsymbol{I}+\boldsymbol{O})(\boldsymbol{I}-\boldsymbol{O})$ which can reduce the iteration times from $K_j = 2^k$ to k. Then, Eq. (22) is transformed into the equation as follows

$$\boldsymbol{P}_j \begin{Bmatrix} \boldsymbol{u}_j(y_l) \\ \boldsymbol{t}_j(y_l) \end{Bmatrix} = \boldsymbol{Q}_j \begin{Bmatrix} \boldsymbol{u}_j(y_u) \\ \boldsymbol{t}_j(y_u) \end{Bmatrix} + \boldsymbol{U}_j \tag{23}$$

where $\boldsymbol{u}_j(y_l)$, $\boldsymbol{t}_j(y_l)$ and $\boldsymbol{u}_j(y_u)$, $\boldsymbol{t}_j(y_u)$ denote the displacement and traction on the lower and upper surface of the jth layer, respectively.

4. State space boundary element method

Let's take a three-layered laminated structure shown in Fig. 2 for instance to explain the establishment of the state space boundary element method. The laminated structure is divided into two parts, in which the 1st layer is the BEM domain and the others are in the range of the

SSM domain.

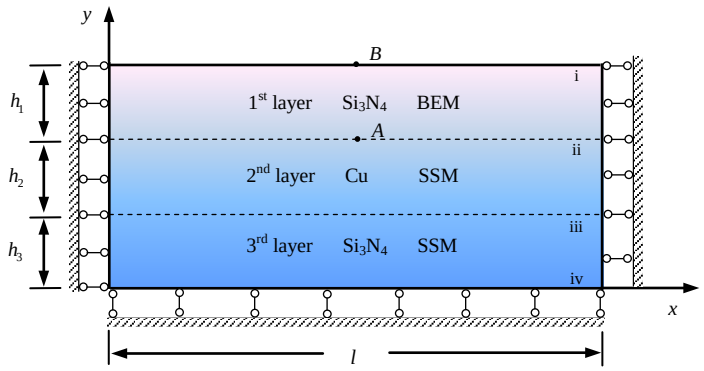

Fig.2 BEM and SSM domain in the state space boundary element method

In Fig. 2, the notation i and iv denote the upper and lower edge, respectively. ii and iii denote the interface between two adjacent layers, respectively. For the BEM domain, the linear equation system can be formed on the basis of Eq.(4) and written as

$$\begin{bmatrix}\boldsymbol{H}_1^{\mathrm{B}} & \boldsymbol{H}_2^{\mathrm{B}}\end{bmatrix}\begin{Bmatrix}\boldsymbol{u}_{\mathrm{OB}}^{\mathrm{B}}\\ \boldsymbol{u}_{\mathrm{ii}}^{\mathrm{B}}\end{Bmatrix}=\begin{bmatrix}\boldsymbol{G}_1^{\mathrm{B}} & \boldsymbol{G}_2^{\mathrm{B}}\end{bmatrix}\begin{Bmatrix}\boldsymbol{t}_{\mathrm{OB}}^{\mathrm{B}}\\ \boldsymbol{t}_{\mathrm{ii}}^{\mathrm{B}}\end{Bmatrix} \tag{24}$$

where the superscript B means that the corresponding component is in the BEM domain, the subscript OB denotes the outer boundary of the BEM domain. On basis of Eq.(23), the thermal elasticity state space equation for the second and third layer can be respectively expressed as

$$\begin{bmatrix}\boldsymbol{Q}_1^{\mathrm{S}} & \boldsymbol{Q}_2^{\mathrm{S}}\end{bmatrix}\begin{Bmatrix}\boldsymbol{u}_{\mathrm{ii}}^{\mathrm{S}}\\ \boldsymbol{t}_{\mathrm{ii}}^{\mathrm{S}}\end{Bmatrix}=\begin{bmatrix}\boldsymbol{P}_1^{\mathrm{S}} & \boldsymbol{P}_2^{\mathrm{S}}\end{bmatrix}\begin{Bmatrix}\boldsymbol{u}_{\mathrm{iii}}^{\mathrm{S}}\\ \boldsymbol{t}_{\mathrm{iii}}^{\mathrm{S}}\end{Bmatrix}-\boldsymbol{U}_2 \tag{25a}$$

$$\begin{bmatrix}\boldsymbol{Q}_3^{\mathrm{S}} & \boldsymbol{Q}_4^{\mathrm{S}}\end{bmatrix}\begin{Bmatrix}\boldsymbol{u}_{\mathrm{iii}}^{\mathrm{S}}\\ \boldsymbol{t}_{\mathrm{iii}}^{\mathrm{S}}\end{Bmatrix}=\begin{bmatrix}\boldsymbol{P}_3^{\mathrm{S}} & \boldsymbol{P}_4^{\mathrm{S}}\end{bmatrix}\begin{Bmatrix}\boldsymbol{u}_{\mathrm{iv}}^{\mathrm{S}}\\ \boldsymbol{t}_{\mathrm{iv}}^{\mathrm{S}}\end{Bmatrix}-\boldsymbol{U}_3 \tag{25b}$$

where the superscript S means that the corresponding parameter is in the SSM domain.

By utilizing the continuity conditions at the interface between the BEM domain and SSM domain

$$\boldsymbol{u}_{\mathrm{ii}}^{\mathrm{B}}=\boldsymbol{u}_{\mathrm{ii}}^{\mathrm{S}},\quad \boldsymbol{t}_{\mathrm{ii}}^{\mathrm{B}}=\boldsymbol{t}_{\mathrm{ii}}^{\mathrm{S}} \tag{26}$$

to combine Eq.(24) and Eq.(25), the state space boundary element equation of a laminated structure can be finally written as follows

$$\begin{bmatrix}\boldsymbol{H}_1^{\mathrm{B}} & \boldsymbol{H}_2^{\mathrm{B}} & -\boldsymbol{G}_2^{\mathrm{B}} & 0 & 0 & 0 & 0\\ 0 & \boldsymbol{Q}_1^{\mathrm{S}} & \boldsymbol{Q}_2^{\mathrm{S}} & -\boldsymbol{P}_1^{\mathrm{S}} & -\boldsymbol{P}_2^{\mathrm{S}} & 0 & 0\\ 0 & 0 & 0 & \boldsymbol{Q}_3^{\mathrm{S}} & \boldsymbol{Q}_4^{\mathrm{S}} & -\boldsymbol{P}_3^{\mathrm{S}} & -\boldsymbol{P}_4^{\mathrm{S}}\end{bmatrix}\begin{Bmatrix}\boldsymbol{u}_{\mathrm{OB}}^{\mathrm{B}}\\ \boldsymbol{u}_{\mathrm{ii}}^{\mathrm{B}}\\ \boldsymbol{t}_{\mathrm{ii}}^{\mathrm{B}}\\ \boldsymbol{u}_{\mathrm{iii}}^{\mathrm{S}}\\ \boldsymbol{t}_{\mathrm{iii}}^{\mathrm{S}}\\ \boldsymbol{u}_{\mathrm{iv}}^{\mathrm{S}}\\ \boldsymbol{t}_{\mathrm{iv}}^{\mathrm{S}}\end{Bmatrix}=\boldsymbol{G}_1^{\mathrm{B}}\begin{Bmatrix}\boldsymbol{t}_{\mathrm{OB}}^{\mathrm{B}}\\ 0\\ 0\end{Bmatrix}-\begin{Bmatrix}0\\ \boldsymbol{U}_2\\ \boldsymbol{U}_3\end{Bmatrix} \tag{27}$$

The unknown physical quantity on the outer boundary at BEM domain and the one on all interfaces can be yielded after Eq.(27) being solved. Then, the displacement and stress of near boundary interior point in the BEM domain can be accurately evaluated by introducing the analytical formulation to the boundary integral equation.

5. Numerical examples

5.1 A sandwich structure

Let's take a three-layered sandwich structure shown in Fig. 2 into consideration. The first and third layer are set as Si_3N_4, whose elastic modulus is 3.04×10^{11}Pa, Poisson's ratio is 0.27 and thermal expansion coefficient is $2.8\times10^{-6}/^{\circ}$C. The second layer is set as Cu, whose elastic modulus is 1.08×10^{11}Pa, Poisson's ratio is 0.33 and thermal expansion coefficient is $1.64\times10^{-5}/^{\circ}$C. The length and thickness of the structure respectively are $l=1$m and $w=0.01$m. $h_2=h_3=0.5$m and h_1 is kept decreasing. It will lead to the nearly singular integral in the SSBEM when h_1 is small. The elasticity problem and thermal elasticity problem are respectively considered here. In the elasticity problem, the uniform pressure $p=1\times10^{8}$N/m^2 is loaded on the upper surface of the first layer. In the thermal elasticity problem, the temperature loading $\Delta T=1\ ^{\circ}$C is subjected.

The physical quantities of interfacial point $A(0.5\text{m},1\text{m})$ with different h_1 are calculated by three different methods. The first one is the conventional SSBEM abbreviated as CSSBEM, in which the nearly singular integral is calculated with Gaussian's quadrature. The second one is the analytical SSBEM abbreviated as ASSBEM, in which the analytical formulation is applied to evaluate the nearly singular integral. The third one is the finite element method, which is introduced to provide the reference result.

The vertical edges are restrained along the *x*-axis and the bottom edge is restrained along the *y*-axis. For the CSSBEM and ASSBEM, 20 elements with each length 0.05m are discretized on each interface and horizontal edge. The left and right vertical edges in the BEM domain are discretized respectively by 2 linear elements and the whole structure is meshed with 84 linear elements in total. For the FEM, 8-node quadratic plane element is implemented in the FEM software ANSYS (Version 10.0). In order to harmonize the element size in vertical and horizontal direction in the FEM, the element number thus increases dramatically as the 1st layer's height h_1 decreases. Due to the limitation of Boolean operation tolerance in ANSYS, the FEM can only model the cases when $h_1\geq5.0\text{e-}4$m. Meanwhile, there are totally 26000 elements and 78481 nodes when $h_1=5.0\text{e-}4$m in the FEM model.

For the elasticity problem, the comparison of quantities at point A by three different methods is listed in Table 1, from which it can be concluded that the results by the ASSBEM and CSSBEM have a good agreement with the one by the FEM. The results of displacement and stress by the ASSBEM keep steady from $h_1 = 0.05\text{m}$ to $h_1 = 5.0\text{e-}8\text{m}$. However, the results by the CSSBEM deteriorate when $h_1 = 5.0\text{e-}5\text{m}$.

Table 1 Displacement and stress at point *A* in elasticity problem

h_1(m)	u_y ($\times 10^{-2}$mm)			σ_{xx} (MPa)		
	ASSBEM	CSSBEM	FEM	ASSBEM	CSSBEM	FEM
5.0e-02	-0.565	-0.565	-0.565	-27.00	-27.00	-27.00
2.5e-02	-0.565	-0.565	-0.565	-27.00	-26.99	-27.00
5.0e-03	-0.565	-0.565	-0.565	-27.00	-27.03	-27.00
5.0e-04	-0.565	-0.565	-0.565	-27.00	-27.04	-27.00
5.0e-05	-0.565	-0.566	/	-27.00	-30.23	/
5.0e-06	-0.565	-0.743	/	-27.00	/	/
5.0e-07	-0.565	/	/	-27.00	/	/
5.0e-08	-0.565	/	/	-27.00	/	/

For the thermal elasticity problem, the physical quantities at interfacial point A calculated by three methods are compared in Table 2. Due to the computational limitation, the ANSYS can only analyze the structure for $h_1 \geq 5.0\text{e-}4\text{m}$. It can be observed from Table 2 that the result from the ASSBEM keeps steady from $h_1 = 0.05\text{m}$ to $h_1 = 5.0\text{e-}9\text{m}$, however, the CSSBEM can only obtain accurate results when $h_1 \geq 5.0\text{e-}5\text{m}$.

Table 2 Displacement and stress at point A in thermal elasticity problem

h_1(m)	u_y ($\times 10^{-2}$mm)			σ_{xx} (MPa)		
	ASSBEM	CSSBEM	FEM	ASSBEM	CSSBEM	FEM
5.0e-02	1.2684	1.2684	1.2684	-85.12	-85.12	-85.12
2.5e-02	1.2684	1.2684	1.2684	-85.12	-85.12	-85.12
5.0e-03	1.2684	1.2684	1.2684	-85.12	-85.12	-85.12
5.0e-04	1.2684	1.2684	1.2684	-85.12	-85.12	-85.12
5.0e-05	1.2684	1.2687	/	-85.12	-85.11	/
5.0e-06	1.2684	1.3358	/	-85.12	-82.59	/
5.0e-07	1.2684	/	/	-85.12	/	/

5.0e-08	1.2684	/	/	-85.12	/	/
5.0e-09	1.2684	/	/	-85.12	/	/

To investigate the evaluation ability of nearly singular integral, h_1 is set as 0.5m, and let y-coordinate of the inner point approach to the boundary.

For the elasticity problem, the displacement u_y and stress σ_{xx} at different inner point (0.5m, y) obtained by the ASSBEM, CSSBEM and FEM are listed in Table 3, where the displacement and stress at boundary point $B(0.5\text{m},1.5\text{m})$ are listed at the bottom line. The physical quantity of the interior point will converge towards the one at boundary point B when it is approaching to the boundary. For the CSSBEM, the stress is invalid when $y=1.475\text{m}$ and the vertical displacement loses the accuracy when $y=1.495\text{m}$. On the contrary, the results by ASSBEM approximately equal to the boundary value when the inner point is very close to the boundary.

Table 3 Displacement and stress at near boundary inner point in elasticity problem

y(m)	u_y ($\times 10^{-2}$mm)			σ_{xx} (MPa)		
	ASSBEM	CSSBEM	FEM	ASSBEM	CSSBEM	FEM
1.400000	-0.687	-0.687	-0.687	-27.00	-27.00	-27.00
1.450000	-0.702	-0.702	-0.702	-26.99	-26.99	-27.00
1.475000	-0.710	-0.709	-0.710	-27.00	-39.81	-27.00
1.490000	-0.715	-0.727	-0.714	-27.00	/	-27.00
1.495000	-0.716	-0.731	-0.716	-27.00	/	-27.00
1.497500	-0.717	-0.596	/	-27.00	/	/
1.499500	-0.717	/	/	-27.00	/	/
1.499750	-0.717	/	/	-27.00	/	/
1.499950	-0.718	/	/	-27.00	/	/
1.499995	-0.718	/	/	-27.65	/	/
1.500000	-0.718	-0.718	-0.718	-27.00	-27.00	-27.00

For the thermal elasticity problem, u_y and σ_{xx} of different inner point (0.5m, y) are listed in Table 4, from which it can be observed that the thermal displacement by the CSSBEM is invalid when y is smaller than 1.495m, and the thermal stress loses accuracy when y is smaller than 1.45m. On the contrary, the results by the ASSBEM are accurate and stable because they

converge to the values of boundary point $B(0.5\text{m},1.5\text{m})$.

Table 4 Displacement and stress at near boundary inner point in thermal elasticity problem

y(m)	u_y ($\times 10^{-2}$mm)			σ_{xx} (MPa)		
	ASSBEM	CSSBEM	FEM	ASSBEM	CSSBEM	FEM
1.400000	1.4106	1.4106	1.4106	-85.12	-85.12	-85.12
1.450000	1.4284	1.4284	1.4284	-85.14	-85.14	-85.12
1.475000	1.4373	1.4364	1.4373	-85.12	-59.42	-85.12
1.490000	1.4426	1.4681	1.4426	-85.13	/	-85.12
1.495000	1.4444	1.4742	1.4444	-85.12	/	-85.12
1.497500	1.4453	1.2018	/	-85.11	/	/
1.499500	1.4460	/	/	-85.11	/	/
1.499750	1.4461	/	/	-85.11	/	/
1.499950	1.4462	/	/	-85.11	/	/
1.499995	1.4462	/	/	-83.77	/	/
1.500000	1.4462	1.4462	1.4462	-85.12	-85.12	-85.12

5.2 A functionally graded material structure

The functionally graded material (FGM) is delaminated as an 11-layered structure shown in Fig. 1, except that the 1st layer is controlled by the BEM, the other 10 layers are set as the SSM domain. The length, height and thickness of each layer are set as 1m, 0.1m and 0.01m, respectively. The elastic modulus varies as the function $E(i)=2^{4(1.1-y_u^i)}\times 10^{11}\,\text{Pa}$ and the thermal expansion coefficient of each layer varies as $\alpha(i)=i\times 10^{-7}/^{\circ}\text{C}$, where i denotes the ith layer. The Poisson's ratio of each layer is set as 0.3. The vertical edges are restrained along the x-axis and the bottom edge is restrained along the y-axis. The whole structure is subjected to $1\,^{\circ}\text{C}$ temperature increase. The contour plot of displacement u_y by the ASSBEM and FEM are compared in Fig. 3.

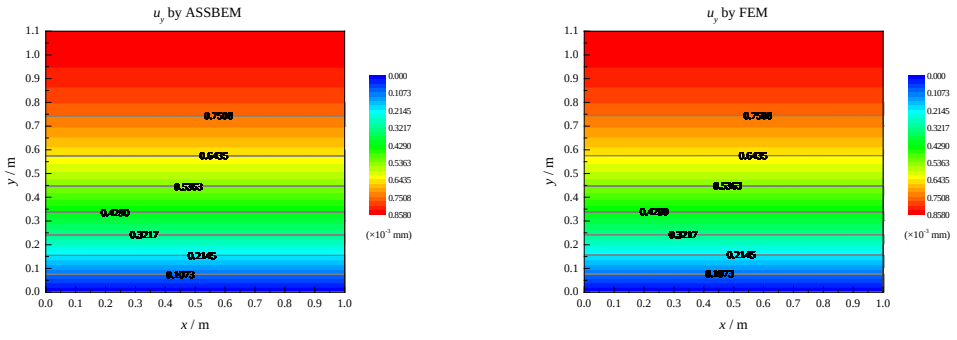

Fig.3 Comparison of contour plot of displacement u_y by ASSBEM and FEM

It can be observed from Fig. 3 that the results by the ASSBEM agree well with the ones by the FEM. The structure can freely expand along the *y*-axis according to the boundary condition. It can be deduced that the maximum vertical displacement should appear on the upper edge. Definitely, the maximum vertical displacement occurs on the upper edge in Fig. 3, which is 0.858×10^{-3} mm.

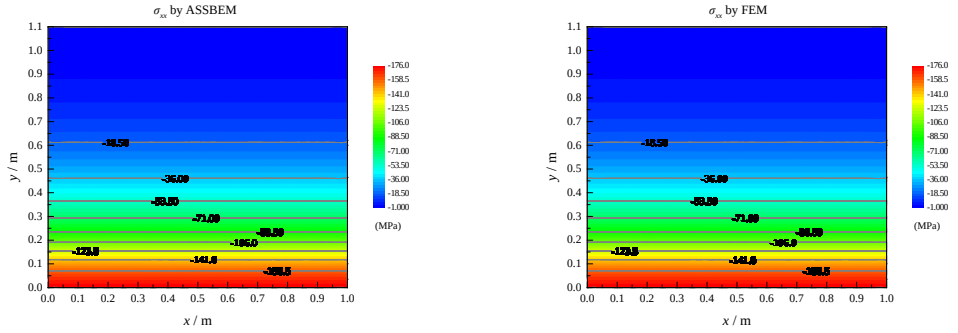

Fig.4 Comparison of contour plot of stress σ_{xx} by ASSBEM and FEM

The contour plot of stress σ_{xx} obtained by ASSBEM is compared with the one by FEM in Fig. 4, from which it can be observed that the results by these two methods have a good agreement with each other. It also can be found that the absolute σ_{xx} decreases along *y*-axis since the thermal expansion coefficient gets smaller in this direction. The absolute minimum σ_{xx} occurs on the upper edge which is $1\,\text{MPa}$, while the absolute maximum σ_{xx} appears on the bottom which is $176\,\text{MPa}$.

6. Conclusions

The state space boundary element method is established by coupling the state space method and the boundary element method, in which the analytical formulation of nearly singular integral is introduced. It is especially suitable for calculating the mechanical quantity of the near boundary inner point in the laminated structure. The accuracy of the present method is verified by the finite element method. The present results for the displacement and stress at near boundary inner point are approaching to the boundary values when the ANSYS fails to provide the reference results.

Acknowledgments

This work was supported by the National Natural Science Foundation of China, China (No.11372094).

References

[1] Fan, J. R., Ye, J. Q. (1990) An exact solution for the statics and dynamics of laminated thick plates with orthotropic layers, *International Journal of Solids and Structures* **26**, 655-662.

[2] Attallah, K. M. Z., Ye, J. Q., Sheng, H. Y. (2007) Three-dimensional finite strip analysis of laminated panels, *Computers & Structures* **85**, 1769-1781.

[3] Attallah, K. M. Z., Yu, M., Ye, J. Q. (2014) Three-dimensional state space spline finite strip analysis of angle-plied laminates, *Composites Part B: Engineering* **66**, 25-35.

[4] Khezri, M., Gharib, M., Bradford, M. A., Vrcelj, Z. (2015) Analysis of thick and orthotropic rectangular laminated composite plates using a state-space-based generalised RKP-FSM, *Composite Structures* **133**, 691-706.

[5] Sheng, H. Y., Ye, J. Q. (2002) A semi-analytical finite element for laminated composite plates, Composite Structures **57**, 117-123.

[6] Sheng, H. Y., Ye, J. Q. (2002) A state space finite element for laminated composite plates, *Computer Methods in Applied Mechanics and Engineering* **191**, 4259-4276.

[7] Ye, J. Q., Sheng, H. Y., Qin, Q. H. (2004) A state space finite element for laminated composites with free edges and subjected to transverse and in-plane loads, *Computers & structures* **82**, 1131-1141.

[8] Jodaei, A., Jalal, M., Yas, M. H. (2012) Free vibration analysis of functionally graded annular plates by state-space based differential quadrature method and comparative modeling by ANN, *Composites Part B: Engineering* **43**, 340-353.

[9] Wu, C. P., Jiang, R. Y. (2012) A state space differential reproducing kernel method for the 3D analysis of FGM sandwich circular hollow cylinders with combinations of simply-supported and clamped edges, *Composite Structures* **94**, 3401-3420.

[10] Sheng, H. Y., Ye, J. Q. (2005) State space solution for axisymmetric bending of angle-ply laminated cylinder with clamped edges, *Composite structures* **68**, 119-128.

[11] Khezri, M., Gharib, M., Bradford, M. A., Uy, B. (2015) A state space augmented generalised RKPM for three-dimensional analysis of thick and laminated composite plates, *Composite structures* **158**, 225-239.

[12] Gu, J., Zhang, J., Li, G. (2012) Isogeometric analysis in BIE for 3-D potential problem, *Engineering Analysis with Boundary Elements* **36**, 858-865.

[13] Simpson, R. N., Bordas, S. P. A., Trevelyan, J., Rabczuk, T. (2012) A two-dimensional isogeometric boundary element method for elastostatic analysis, *Computer Methods in Applied Mechanics and Engineering* **209**, 87-100.

[14] Zheng, B., Gao, X., Zhang, C. (2016) Radial integration BEM for vibration analysis of two-and three-dimensional elasticity structures, *Applied Mathematics and Computation* **277**, 111-126.

[15] Tsiatas, G. C., Yiotis, A. J. (2013) A BEM-based meshless solution to buckling and vibration problems of orthotropic plates, *Engineering Analysis with Boundary Elements* **37**, 579-584.

[16] Zhang, Y. M., Gu, Y., Chen, J. T. (2011) Stress analysis for multilayered coating systems using semi-analytical BEM with geometric non-linearlyities, *Computational Mechanics* **47**, 493-504.

[17] Cheng, C., Han, Z., Yao, S., Niu, Z., Recho, N. (2014) Analysis of heat flux singularity at 2D notch tip by singularity analysis method combined with boundary element technique, *Engineering Analysis with Boundary Elements* **46**, 1-9.

[18] Aour, B., Rahmani, O., Nait-Abdelaziz, M. (2007) A coupled FEM/BEM approach and its accuracy for solving crack problems in fracture mechanics, *International Journal of Solids and Structures* **44**, 2523-2539.

[19] Padrón, L. A., Aznárez, J. J., Maeso, O. (2007) BEM-FEM coupling model for the dynamic analysis of piles and pile groups, *Engineering Analysis with Boundary Elements* **31**, 473-484.

[20] Bonnet, G., Seghir, A., Corfdir, A. (2009) Coupling BEM with FEM by a direct computation of the boundary stiffness matrix, *Computer Methods in Applied Mechanics and Engineering* **198**, 2439-2445.

[21] Benedetti, I., Aliabadi, M. H., Milazzo, A. (2010) A fast BEM for the analysis of damaged structures with bonded piezoelectric sensors, *Computer Methods in Applied Mechanics and Engineering* **199**,

490-501.

[22] Lin, C. C., Lawton, E. C., Caliendo, J. A., Anderson, L. R. (1996) An iterative finite element-boundary element algorithm, *Computers & Structures* **59**, 899-909.

[23] Boumaiza, D., Aour, B. (2014) On the efficiency of the iterative coupling FEM–BEM for solving the elasto-plastic problems, *Engineering Structures* **72**, 12-25.

[24] Njiwa, R. K., Niane, N. T., Frey, J., Schwartz, M., Bristiel, P. (2015) A coupling strategy of FEM and BEM for the solution of a 3D industrial crack problem, *International Journal for Computational Methods in Engineering Science and Mechanics* **16**, 112-120.

[25] Niu, Z. R., Cheng, C. Z., Zhou, H. L., Hu, Z. J. (2007) Analytic formulations for calculating nearly singular integrals in two-dimensional BEM, *Engineering Analysis with Boundary Elements* **31**, 949-964.

[26] Zhong, W. X., Williams, F. W. (1994) A precise time step integration method, *Proceedings of the Institution of Mechanical Engineers, Part C: Journal of Mechanical Engineering Science* **208**, 427-430.